

# Soviet superalloy ZHS6-K, effect of B/C modification

S. N. TEWARI, M. HEMAREDDY

*Defence Metallurgical Research Laboratory, PO Kanchanbagh, Hyderabad 500 258, India*

A Soviet nickel base cast superalloy, ZHS6-K, has been examined for its response to B/C modification. Three alloy chemistry variants, with 0.17C/0.02B, 0.06C/0.1B and 0.03C/0.2B (wt %) have been investment cast and investigated for microstructure, heat-treatment, tensile properties, stress-rupture properties and hot corrosion resistance. The B/C modification of the alloy results in some improvement in the yield strength. However, the tensile ductility and the stress-rupture properties are considerably degraded. The nature of the hot corrosion is of a pitting type for the ZHS6-K, whereas it is of a broad front type for the high boron alloys.

## 1. Introduction

An alloy chemistry modification (the so-called B/C concept), increased boron and decreased carbon, has been reported to improve the castability [1, 2], the intermediate temperature tensile ductility [3, 4], and stress-rupture life, and to reduce the scatter in mechanical properties due to the decreased porosity for several nickel base cast superalloys. Several well known nickel base superalloys, including IN-792, IN-738, and MM-200, [1, 3, 5] have been modified in this manner with a generally improved performance. Nickel base superalloys with a relatively high cobalt content have traditionally been used to fabricate the investment cast gas turbine blade and vane components. A very steep rise in the cobalt price over the past few years has forced a re-examination of the role of cobalt in cast superalloys to find alternatives to this element [6]. Soviet superalloys generally contain less cobalt as compared to their equivalent western counterparts, e.g. 4.5 wt % in ZHS6-K [7] against 15 wt % in IN-100 [8]. The purpose of this investigation was to examine the response of a low cobalt advanced nickel base Soviet superalloy, ZHS6-K, to such B/C modification. In this investigation B/C modified ZHS6-K alloys have been examined with respect to their microstructure, heat-treatment, temperature dependence of the tensile properties, stress-rupture properties and hot-corrosion resistance.

## 2. Experimental procedure

Three carbon and boron chemistry variants, i.e. 0.17C/0.02B, 0.06C/0.1B, and 0.03C/0.2B, were prepared for the same nominal base alloy composition of Ni-11.5% Cr-5% W-4.5% Co-4% Mo-2.9% Ti-6% Al (wt %). The alloys were prepared by melting a 6 kg charge consisting of master alloys, such as, nickel-boron and iron-tungsten, and pure elements, such as nickel, chromium, molybdenum, cobalt, titanium, aluminium and carbon in a vacuum induction melting furnace. The melts were vacuum poured at 1500°C into preheated zircon investment shell moulds to obtain 8 investment cast bars (1.25 cm diameter × 10 cm long). Some of these bars were heat treated in air, 1200°C/2 h aircool + 1000°C/24 h aircool.

Tensile (gauge diameter = 4 mm, gauge length = 26 mm) and stress rupture (gauge diameter = 3 mm, gauge length = 15 mm) specimens were machined from both the investment cast and the heat treated bars, and were inspected by X-ray radiography. Tensile tests were conducted in air at room temperature, 500, 700, 800, 900 and 1000°C at a crosshead speed of 0.1 cm min<sup>-1</sup>. Stress-rupture tests were carried out in air at 800°C and 53 kg mm<sup>-2</sup>, and 900°C and 33 kg mm<sup>-2</sup>.

The microstructures were examined by optical and electron replica/transmission metallography.

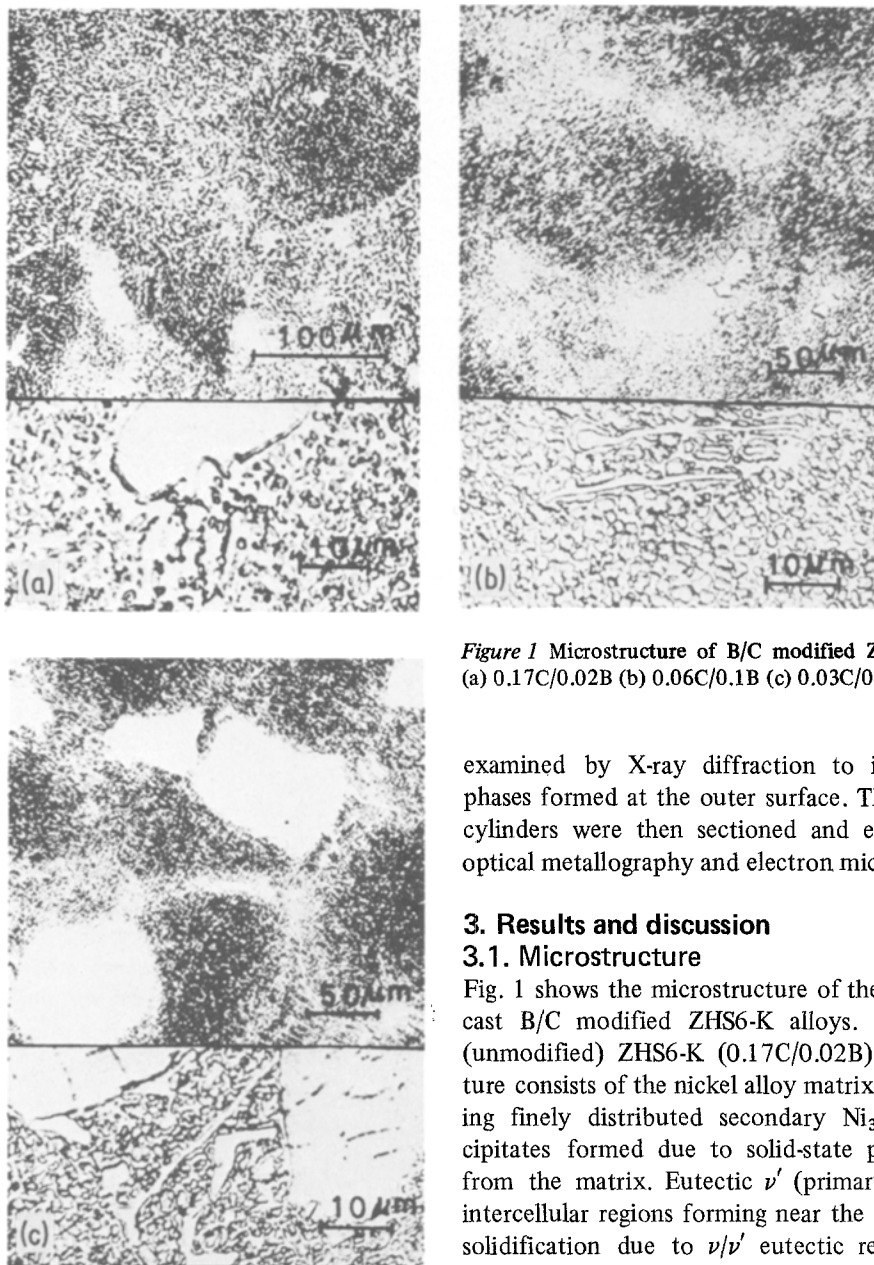


Figure 1 Microstructure of B/C modified ZHS6-K alloys (a) 0.17C/0.02B (b) 0.06C/0.1B (c) 0.03C/0.2B.

examined by X-ray diffraction to identify the phases formed at the outer surface. The specimen cylinders were then sectioned and examined by optical metallography and electron microprobe.

### 3. Results and discussion

#### 3.1. Microstructure

Fig. 1 shows the microstructure of the investment cast B/C modified ZHS6-K alloys. The regular (unmodified) ZHS6-K (0.17C/0.02B) microstructure consists of the nickel alloy matrix ( $\nu$ ) containing finely distributed secondary  $Ni_3X$  ( $\nu'$ ) precipitates formed due to solid-state precipitation from the matrix. Eutectic  $\nu'$  (primary  $\nu'$ ) in the intercellular regions forming near the end of alloy solidification due to  $\nu/\nu'$  eutectic reaction, and primary MC type carbide precipitates are also present in the base alloy. Increasing amount of boron addition results in the appearance of two types of borides. One is blocky and appears more in the centres of dendrites. The other is lamellar-like and appears to have formed as a eutectic between  $\nu$  and boride in the inter-dendritic regions. The volume fraction of these boride regions increases with the increasing boron content. Both types of borides are enveloped with the secondary  $\nu'$  precipitates due to the ease of  $\nu'$  nucleation and growth there. The eutectic  $\nu'$  particles have long lamellar type borides associated with them at their

X-ray images of the elemental distributions in the microstructure were obtained by the use of an electron microprobe.

Hot corrosion crucible tests [9] were conducted on cylindrical specimens (8 mm in diameter  $\times$  5 mm long) machined and ground to a fine surface finish (no. 600 emery paper). These cylinders were half immersed for 20 h in a salt mixture consisting of 96% sodium sulphate and 4% sodium chloride kept in a quartz crucible at 850° C. The hot corroded surface after washing in distilled water was

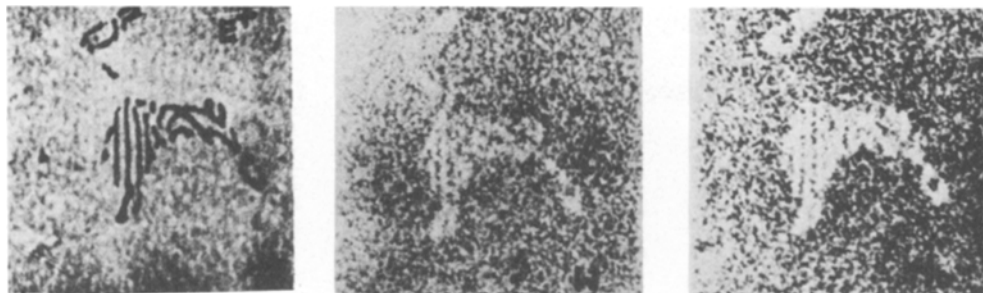


Figure 2 Electron microprobe X-ray image of the eutectic borides.

surface (Fig. 1c), whereas the  $\nu$ -boride eutectic regions do not have eutectic  $\nu'$  associated with them. This suggests that the  $\nu/\nu'$  eutectic formation temperature is higher than the  $\nu$ -boride eutectic formation temperature. The volume fraction of the eutectic  $\nu'$  region increases with the increasing boron content of the alloy. The borides are rich in tungsten and molybdenum (Fig. 2). Similar "script type" borides have been earlier reported to be rich in chromium, titanium and molybdenum [8]. However, the borides in this alloy do not show any enrichment of chromium and titanium. The amount of titanium which is generally locked up in forming MC type carbides in the unmodified alloy is available, therefore, to form more of the eutectic  $\nu'$  regions in the B/C modified alloys. The precipitates formed in the eutectic regions due to solid-state precipitation are much more pronounced in the 0.2B/0.03C alloy than the unmodified one.

Microstructural examination of the specimens after a 2 h heat treatment at a 25° C temperature interval from 1100 to 1250° C followed by air cooling to room temperature showed that the secondary  $\nu'$  precipitates begin to dissolve at about 1150° C, preferably in the intercellular regions. However, a complete  $\nu'$  solutioning occurs only at 1200° C. 1250° C exposure results in incipient melting in the regions containing the  $\nu$ -boride eutectics. The eutectic  $\nu'$  regions remained undissolved after the 1200° C exposure. This, however, resulted in partial dissolution of the finger-like boride precipitates resulting in blunting of its sharp edges (Fig. 3). Microstructure of the 0.2B/0.02C alloy after ageing treatments, 900° C for 24 h and 1000° C for 24 h preceded by  $\nu'$  solutioning, 1200° C for 2 h, are shown in Fig. 3. The 900° C ageing results in finer secondary  $\nu'$  precipitates at the cell boundary regions (where finger-like borides were present) and coarser  $\nu'$  within the

cells (Fig. 3a). The 1000° C ageing yields a uniform secondary  $\nu'$  precipitate size distribution (Fig. 3b). It also results in the complete enveloping of the partially dissolved lamellar boride particles by  $\nu'$ . Some fine precipitates appear both in the secondary  $\nu'$  and the  $\nu$  regions of the alloy after this heat treatment (Fig. 3c). They have tentatively been identified to be  $M_3B_2$  as they appear similar to the  $M_3B_2$  precipitates identified earlier in a B/C modified superalloy [5]. The solutioning (1200° C for 2 h + air cooling to room temperature) followed by 1000° C for 24 h + air cooling to room temperature (HT2), therefore, has been used as the heat treatment for the mechanical property investigations. The standard heat treatment reported in literature [7], 1200° C for 4 h + air cool to room temperature (HT1) for ZHS6-K has been used for the 0.17C/0.02B alloy.

### 3.2. Tensile properties

The temperature dependence of the tensile properties for the three alloys investigated is shown in Table I. The ultimate tensile strength (UTS), 0.2% offset yield strength (YS) and per cent elongation (EL) values obtained for the ZHS6-K alloy compare favourably with that reported in literature [7]. The tensile properties of the B/C modified alloys appear generally unchanged due to the heat treatment (HT2). Due to the scatter in the data in Table I, the strength properties of the B/C modified and the ZHS6-K alloys appears to be similar. However, a comparison of the average values obtained for the YS and EL for the heat-treated alloys (Fig. 4) shows that the 0.06C/0.01B alloy generally has the highest yield strength. This advantage must be due to the uniformly distributed fine boride precipitates mentioned earlier providing the strengthening both to the  $\nu$  matrix and the secondary  $\nu'$  precipitates. The 0.03C/0.2B alloy, however, loses some of this

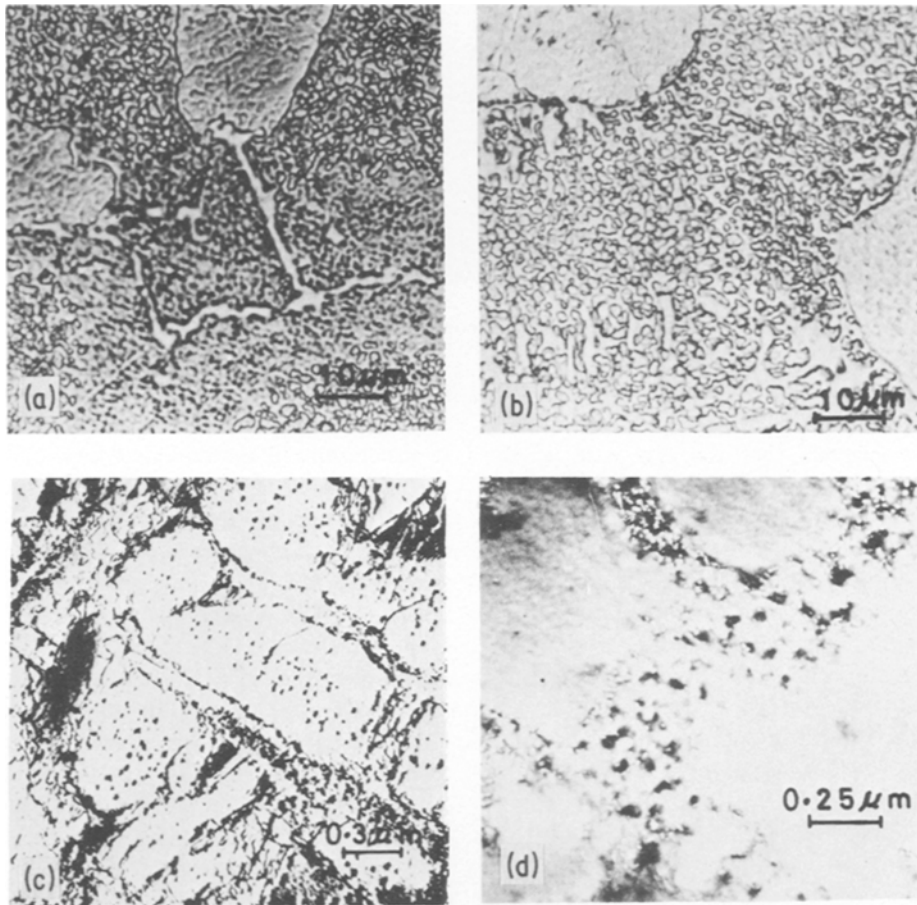


**Figure 3** Effect of heat treatment on the microstructure of the 0.2B/0.03C alloy. (a) 1200°C/2 h + air cool to room temperature + 900°C/24 h + air cool to room temperature. (b) 1200°C/2 h + air cool to room temperature + 1000°C/24 h + air cool to room temperature. (c) Electron micrograph showing the presence of fine borides after the heat treatment “B” above. Precipitates in  $\nu'$  region (bright field image). (d) Electron micrograph showing the presence of fine borides after the heat treatment “B” above. Precipitates in  $\nu'$  region (dark field image).

strengthening advantage due to a much reduced volume fraction of the secondary  $\nu'$  precipitates in the alloy (eutectic  $\nu'$  volume fraction increases at the expense of the secondary  $\nu'$  volume fraction). However, the B/C modified alloys examined also have a much reduced ductility. The microstructural feature responsible for this low ductility is the finger-like eutectic borides. Fig. 5, a cut section through the fracture, shows that the tensile fracture, both at the room temperature and at 800°C is transgranular and intercellular, i.e. the fracture path follows the intercellular regions rich in the eutectic borides. The fracture initiates at the boride matrix interface, either due to the long finger-like eutectic borides in the intercellular regions or due to the long borides precipitated on the eutectic  $\nu'$  nodule surfaces. In both the

B/C modified alloys examined similar fracture behaviour was observed. It appears therefore that by a careful chemistry manipulation the fine uniformly distributed borides should be retained and the finger-like eutectic borides should be avoided to take the strength advantage without suffering from the accompanying ductility loss, as is the case with the two alloy compositions examined.

### 3.3. Stress-rupture properties

The stress-rupture properties of the alloys measured at 800°C and 53 kg mm<sup>-2</sup> and 900°C and 33 kg mm<sup>-2</sup> are given in Table II. The reported rupture life for the heat treated ZHS6-K alloy for the above test conditions is 50 h [7]. The rupture lives obtained for the ZHS6-K alloy (0.17C/0.02B)

T A B L E I Temperature dependence of the tensile properties of B/C ZHS6-K alloys

Alloy C/B (wt %)	Condition	25° C			500° C			700° C			800° C			900° C			1000° C		
		UTS*	YS†	EL‡	UTS	YS	EL	UTS	YS	EL	UTS	YS	EL	UTS	YS	EL	UTS	YS	EL
0.17/0.02	HT1	99.2	80.7	7.2	91.5	77.6	7.4	96.7	79.1	5.1	90.5	83.0	3.4	60.8	52.1	6.1	—	—	—
		83.8	76.1	3.0	91.5	77.6	7.4	83.2	75.1	3.0	84.6	76.0	2.8	59.2	52.0	3.9	—	—	—
		89.6	78.4	5.3	89.2	76.1	7.0	89.4	86.0	0.8	80.3	79.6	0.8	56.2	51.0	2.4	—	—	—
0.06/0.1	AC	99.5	82.6	7.4	87.8	79.2	1.9	—	—	—	—	—	—	—	—	—	—	—	—
		86.5	86.5	0.8	94.7	86.2	1.5	89.2	88.1	0.8	89.2	81.9	1.2	71.4	64.0	0.8	42.3	35.0	3.1
0.03/0.2	HT2	95.9	91.7	2.0	97.2	89.6	1.6	94.2	87.6	0.8	93.2	88.2	1.2	61.5	53.4	3.6	43.1	36.6	2.5
		—	—	—	—	—	—	—	—	—	—	—	—	—	65.5	60.2	2.5	—	—
0.03/0.2	HT2	91.6	89.3	0.5	93.8	87.2	1.0	102.5	93.3	1.4	95.3	88.3	1.5	80.6	70.6	1.6	45.2	35.0	9.7
		89.5	83.8	1.3	95.5	83.8	1.7	97.6	93.8	0.6	87.8	87.8	0.8	65.1	58.3	3.9	42.0	34.3	12.5
0.03/0.2	HT2	89.2	87.6	0.5	—	—	—	92.3	89.7	0.4	—	—	—	66.3	61.3	0.4	46.4	36.8	3.5
		85.4	79.7	0.9	—	—	—	96.8	87.6	1.5	—	—	—	70.7	62.2	2.4	42.8	33.6	3.3

\*UTS: ultimate tensile strength kg mm<sup>-2</sup>.

†YS: 0.2% offset yield strength kg mm<sup>-2</sup>.

‡EL: per cent elongation.

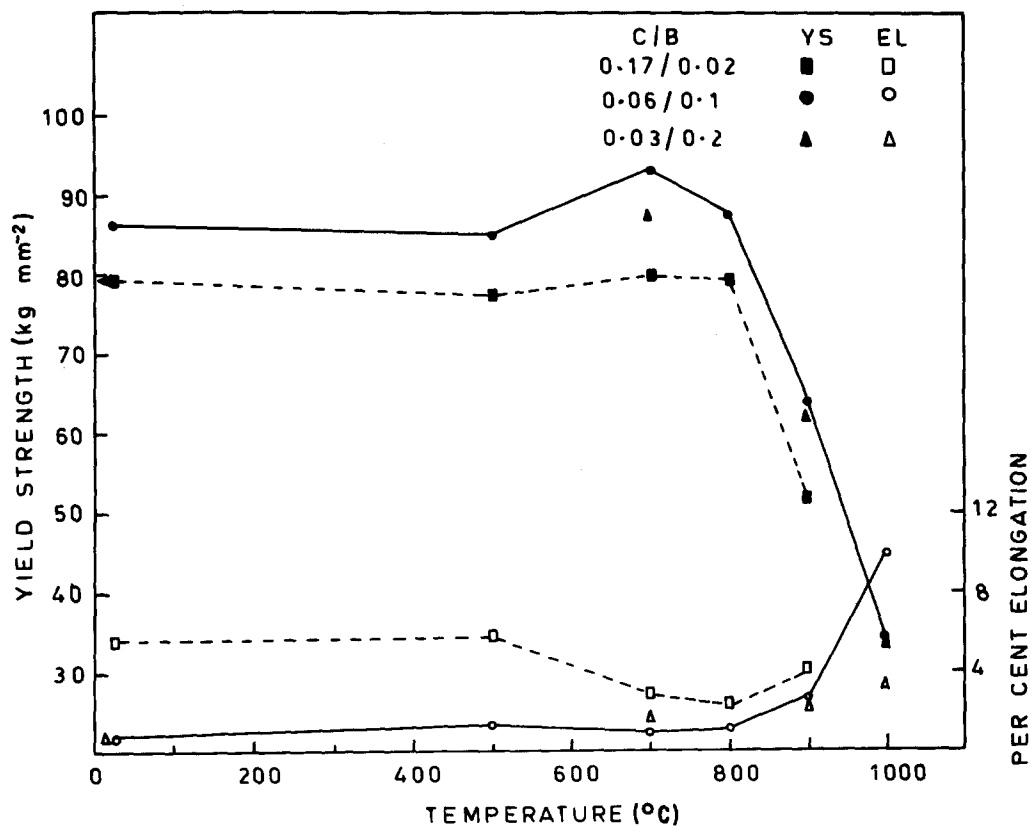


Figure 4 Temperature dependence of the tensile properties for the heat treated B/C modified ZHS6-K alloys.

appear reasonable, except the low life of 25.5 h, which was observed to be due to the casting porosity. The rupture lives of the B/C modified alloys, both in the as-cast and the heat-treated conditions, are generally low despite the fact that both the B/C modified alloy chemistries results in a very good castability and almost total absence of any microporosity. Examination of the fracture surface (Fig. 5c) revealed that the eutectic intercellular borides are responsible for the rupture fracture initiation and propagation. The rupture ductility appears to slightly improve due to the

heat treatment (HT2), possibly due to the blunting of the sharp edges of the long boride precipitates observed earlier (Fig. 3b).

### 3.4. Hot corrosion resistance

A comparison of the hot corrosion behaviour showed that B/C modification results in significant improvement in the alloy resistance. Fig. 6 shows a macroview of the hot corroded specimen cylinders for the ZHS6-K (0.17C/0.02B) and the B/C modified (0.03C/0.2B) alloys. The ZHS6-K alloy has a corrosion product layer which is much more

TABLE II Stress-rupture properties of B/C ZC6-K alloys

Alloy C/B (wt %)	Condition	800° C, 53 kg mm <sup>-2</sup>		900° C, 33 kg mm <sup>-2</sup>	
		Life (h)	%RA	Life (h)	%RA
0.17/0.02	HT1	25.5	1.2	37.2	—
		34.1	1.1	57.5	3.7
0.06/0.1	AC	14.2	0.6	26.4	3.7
		—	—	17.1	1.8
	HT2	20.3	0.6	25.5	1.8
		69.5	1.8	24.6	4.4
0.03/0.2	AC	33.0	—	15.7	—
	HT2	—	—	18.2	—

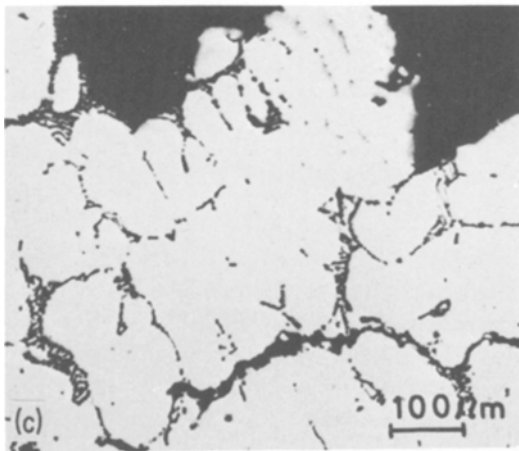
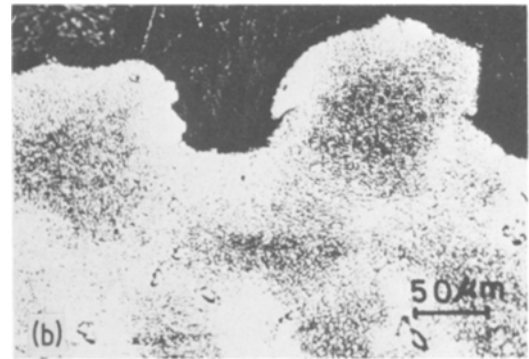
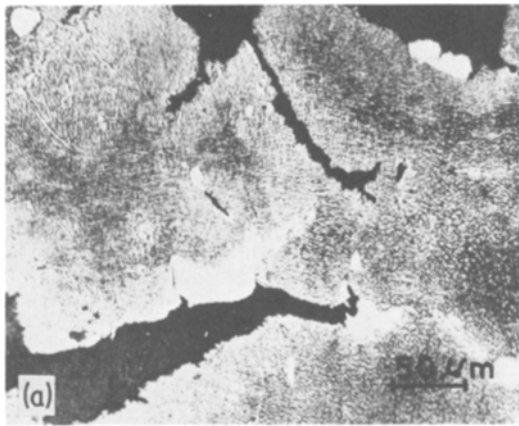


**Figure 5** Fracture behaviour of the B/C modified ZHS6-K alloys (a) Tensile, room temperature, 0.06C/0.1B alloy, HT2, (b) Tensile, 800°C, 0.06C/0.1B alloy, HT2, (c) Stress rupture, 900°C and 33 kg mm<sup>-2</sup>, 0.03C/0.2B alloy, HT2.

porous and has swelled, blistered and cracked. The product layer on the B/C modified alloy is more tenacious. The X-ray diffraction analysis of the hot corroded surface showed the presence of NiO and NiS<sub>2</sub> in the case of ZHS6-K and NiO and Cr<sub>3</sub>S<sub>4</sub> in the case of B/C modified alloy.

The microstructure at the alloy matrix corrosion product interface for the two alloys is shown in Fig. 7. The nature of the corrosion appears to be non-uniform pitting type for the ZHS6-K alloys (Fig. 7a), and is of broad front type for the B/C modified alloy (Fig. 7b). The pitting type



**Figure 6** Macroview of the hot corroded 0.17C/0.02B (left) and 0.03C/0.2B (right) ZHS6-K alloys.

corrosion is expected to be much more detrimental as compared to the broad front type. The carbide precipitates (titanium, tungsten, molybdenum rich) and the eutectic borides (tungsten molybdenum rich) can be seen in the alloy matrices for the two alloys. Cavities where the liquid salt must have been present during corrosion have an access to the alloy matrix surface for the ZHS6-K alloy, whereas such cavities are not present for the B/C modified alloy. Instead, a layer containing porosity and possibly oxides exists between the molten salt and the alloy matrix surface. Even the regions where it appears as if the salt had access to the alloy surface, show the presence of this thin layer at higher magnification (Inset, Fig. 7b).

The sulphur X-ray images for the two alloys at the matrix and corrosion product interface are shown in Fig. 8. The sulphides are of two kinds; one is basically nickel sulphide and the other one contains mainly titanium, chromium and aluminium. Figs. 8c and d, (schematic views based on “S” images) containing the information obtained from the elemental X-ray distributions of sulphur, chromium, titanium, aluminium, cobalt, nickel, tungsten and molybdenum, show the distribution of these sulphides. The sulphides formed in the alloy matrix ahead of the liquid salt are clearly seen for the ZHS6-K alloy, whereas the sulphides formed are not in contact with the B/C modified alloy matrix. The thin layer (containing porosity and possibly oxides) mentioned earlier was found to contain nickel and aluminium.

The location of the corrosion pits was not related to any microstructural feature of the

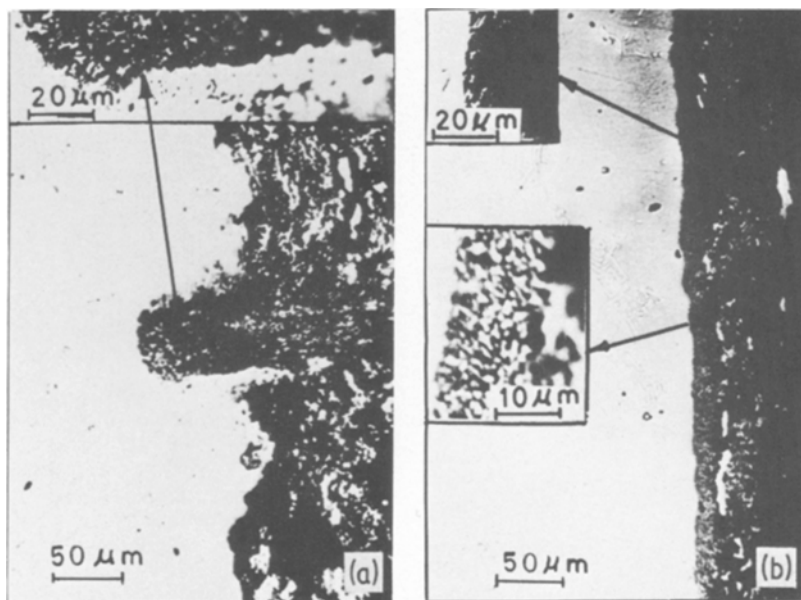


Figure 7 The microstructure at the alloy matrix and hot corrosion product interface. (a) 0.17C/0.02B alloy. (b) 0.03C/0.2B alloy.

ZHS6-K alloy, such as, grain boundary, eutectic  $\nu'$ , carbides, etc. The broad corrosion front in the B/C modified alloy was also not affected by the eutectic borides or eutectic  $\nu'$  lying ahead of it. The major microstructural feature which is different in the B/C modified alloy from the ZHS6-K is the presence of finely distributed boride precipitates in the secondary  $\nu'$  and the  $\nu$  matrix. These precipitates, therefore, must be responsible for changing the hot corrosion process from a non-uniform pitting type to a broad front type.

Hot corrosion of the superalloys is an accelerated corrosion due to the repeated sulphidation and oxidation of the materials. According to the "Fluxing" model [10] the oxide layer forms on the metal surface, the oxide gets dissolved into the salt and reprecipitates at regions away from the salt-oxide interface. In case the oxide film formed on the alloy surface loses its integrity and ruptures, the molten salt gets direct access to the metal surface and a faster degradation of the metal occurs by the formation of sulphides. Boron is a very strong glass forming oxide, with the highest single bond strength value of about  $120 \text{ kcal mol}^{-1}$  for (NiO it is  $30 \text{ kcal mol}^{-1}$ ) and is expected to promote the formation of glassy oxide. In addition some theories of chemical breakdown leading to pitting also postulate film rupture by chemical forces [11], therefore, the ductility of the film is

important. A glassy film is expected to be more ductile than the crystalline film (anodic  $\text{Ta}_2\text{O}_5$  which was glassy lost its ductility after crystallization, [12]). The boron-oxide rich glassy film in the B/C modified alloy must have been more ductile to maintain the continuous oxide film during the hot corrosion. In the case of ZHS6-K the oxide film is of the NiO and  $\text{Cr}_2\text{O}_3$  type, which is expected to be crystalline and brittle. In addition the Ti/Al ratio in  $\nu'$  precipitates is expected to be higher in the B/C modified alloy because the titanium blocked as carbides in ZHS6-K is freed. Higher Ti/Al ratio in  $\nu'$  is expected to lead to a better hot corrosion resistance [13].

#### 4. Conclusions

Examination of the three alloys studied in terms of their microstructure, mechanical properties and hot corrosion resistance suggests that a B/C modified ZHS6-K alloy chemistry should be selected which does not contain the eutectic borides, at the same time has the finely distributed boride precipitates in the matrix and the secondary  $\nu'$  particles. Such an alloy is expected to possess good castability, improved hot corrosion resistance, improved yield strength and possible good rupture strength and alloy ductility.

#### Acknowledgements

Appreciation is expressed to Dr P. Rama Rao,



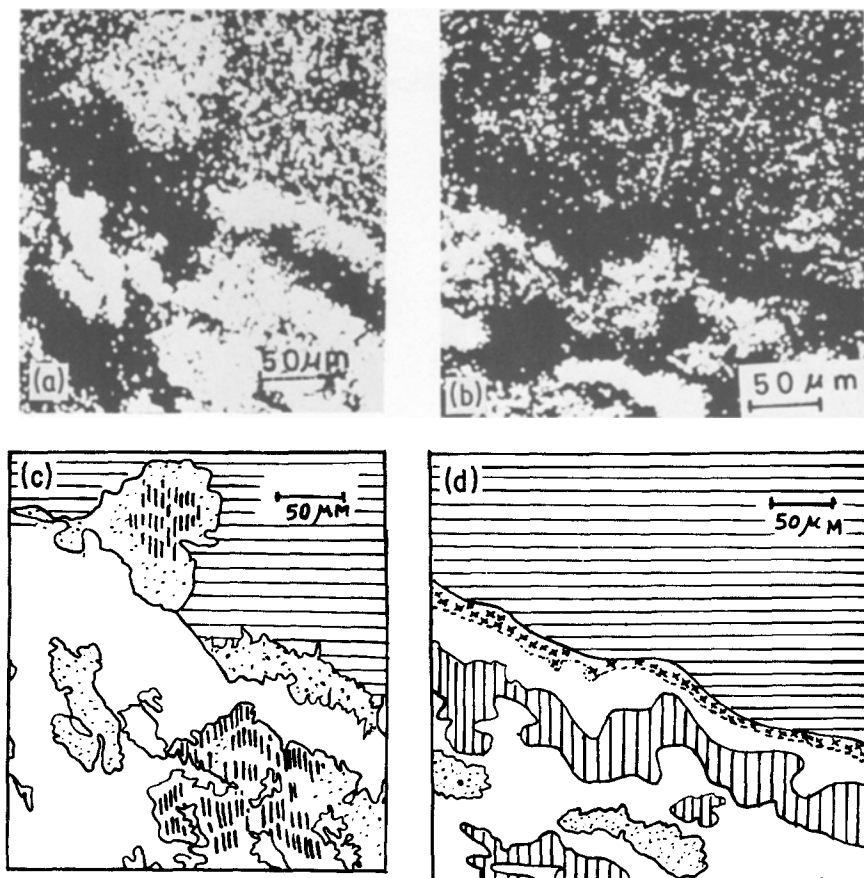
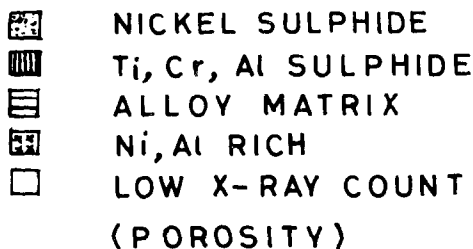


Figure 8 Distribution of the sulphides due to hot corrosion (a) Sulphur X-ray image, 0.17C/0.02B alloy. (b) Sulphur X-ray image, 0.03C/0.2B alloy. (c) Schematic of sulphides in Fig. 8a. (d) Schematic of sulphides in Fig. 8b.



Director, Defence Metallurgical Research Laboratory for his permission to publish this paper.

## References

1. G. L. R. DURBER, "High Temperature Alloys for Gas Turbines" (Applied Science Publishers Ltd., Essex, UK, 1978) p. 459.
2. E. BACHELET and G. LESAULT, "High Temperature Alloys for Gas Turbines" (Applied Science Publishers Ltd, Essex, UK, 1978).
3. C. A. HAMMERSLEY, "Proceedings of the Thirteenth Annual BICTA Conference" (BICTA, Sheffield, UK, 1976) p. 4.1.
4. D. H. MAXWELL, J. E. BALDWIN and J. F. RADAVIDICH, *Metall. Met. Forming* 42 (1975) 332.
5. B. H. KEAR and D. E. FORNWALT, "Superalloy Metallurgy and Manufacture" (Claitors Publishing Division, USA, 1976) p. 265.
6. J. K. TIEN and S. PURUSHOTHAMAN, "Proceedings of the Symposium of Properties of High Temperature Alloys" (Electrochemical Society Inc., Princeton, USA, 1976) p. 12.
7. F. F. KHIMUSHIN, "High Temperature Steels and Alloys" (translation: Foreign Technology Division, Air Force Systems Command, USA, 1970) p. 484.
8. Aerospace Structural Metals Handbook, Vol. 5, Code 4212, (AFML-TR-68-115), (Dept. of Defence, USA, 1977).
9. L. D. GRAHAM, T. D. GADD and R. J. QUIGG, "Hot Corrosion Problems Associated with Gas Turbines" (ASTM Special Technical Publication STP 421, 1976) p. 105.
10. J. STRINGER, "Proceedings of the Symposium on Properties of High Temperature Alloys" (Electrochemical Society Inc., Princeton, USA, 1976) p.513.

11. J. KRUGER, *Nat. Phys. Sci.* **230** (1971) 91.
12. S. F. BUBAR and D. A. VERMILYEA, *J. Electrochem. Sci.* **114** (1967) 882.
13. H. V. DOERING, *J. Mater.* **4** (1969) 457.

*Received 5 April  
and accepted 7 September 1982*